Cardiovascular Engineering and Technology, Vol. 10, No. 2, June 2019 *(© 2019)* pp. 257–270
https://doi.org/10.1007/s13239-019-00403-8

The Impact of the Right Coronary Artery Geometric Parameters on Hemodynamic Performance

N. Pinho,[2] L. C. Sousa,[1,2] C. F. Castro,[1,2] C. C. António,[1,2] M. Carvalho,[4] W. Ferreira,[4] R. Ladeiras-Lopes,[3,4] N. D. Ferreira,[4] P. Braga,[4] N. Bettencourt,[3] and S. I. S. Pinto [1,2]

[1]Engineering Faculty, University of Porto, Rua Dr. Roberto Frias, s/n, 4200-465 Porto, Portugal; [2]Institute of Science and Innovation in Mechanical and Industrial Engineering (LAETA-INEGI), Rua Dr. Roberto Frias, 400, 4200-465 Porto, Portugal; [3]Cardiovascular R&D Unit, Faculty of Medicine, University of Porto, Alameda Prof. Hernâni Monteiro, 4200-319 Porto, Portugal; and [4]Department of Cardiology, Gaia/Espinho Hospital Centre, Rua Conceição Fernandes, s/n, 4434-502 Vila Nova de Gaia, Portugal

(Received 23 October 2018; accepted 28 January 2019; published online 6 February 2019)

Associate Editor Sarah Vigmostad and Ajit P. Yoganathan oversaw the review of this article.

Abstract

Purpose—Coronary artery geometry can have a significant impact in the hemodynamic behavior of coronary blood flow, influencing atherosclerotic plaque formation. The present work focuses on, through a statistical study, the connection between several geometric parameters of the right coronary artery—ostium cross-sectional area, angles between the common trunk and the side-branches, tortuosity, curvature and cross-sectional area in each side-branch—and their influence on hemodynamic descriptors. Parameters such as low wall shear stress and local disturbed flow, which are associated with atherosclerosis formation, were analysed.

Methods—Computed tomography images of ten healthy individuals were selected to reconstruct *in vivo* three-dimensional models of right coronary arteries. Blood flow was simulated through a compliant model with realistic boundary conditions. Calculated hemodynamic descriptors values were correlated with the geometric parameters using the Pearson correlation coefficient (r) and the p value.

Results—The strongest correlations were found in the middle and distal segments of the right coronary artery. A decrease in the ostium area promotes a decrease in the WSS magnitude from the proximal to the distal segment ($r = 0.82$). Very strong correlations ($r > 0.90$) were achieved between geometric parameters (cross-sectional area, angle, tortuosity) of the right-ventricular branch and the wall shear stress magnitude in the middle and distal segments.

Conclusions—Low values of tortuosity, smaller cross-sectional area and higher angle of the right-ventricular branch leads to a hemodynamic behavior more propitious to atherosclerosis formation, within the study cases. The right-ventricular branch seems to have the highest influence in the hemodynamic behavior of the right coronary artery.

Keywords—Atherosclerosis, Right coronary artery, Geometric parameters, Statistics, Fluid–structure interaction, Wall shear stress-based descriptors.

INTRODUCTION

According to the World Health Organization, 7.2 million people die each year from coronary heart disease, being the leading cause of death worldwide.[37] Atherosclerosis is the outcome of the accumulation of lipids and inflammatory response in the inner most layer of the arterial vessel. This accumulation leads to the narrowing of the vessel. When the wall shear stress increases in the narrowed vessel, a rupture may occur, leading to clot formation, vessel occlusion or embolization.[2] Computed tomography (CT) scans provide a clear image of the vessels anatomy and the presence or absence of the atherosclerosis disease. However, they lack the details provided by hemodynamic simulations. The numerical simulations describe blood flow behavior through wall shear stress (WSS) hemodynamic descriptors. The Time-Averaged Wall Shear Stress (TAWSS) lower than 0.4 Pa,[23] the Oscillatory Shear Index (OSI) near 0.5[13,31] (maximum value) and the Relative Residence Time (RRT) higher than 8 Pa^{-1}[19] are considered to be prone regions of atherosclerosis appearance. Moreover, Knight *et al.*[20] found that RRT and OSI provide a lower number of false-positives than TAWSS also widely used.

Address correspondence to S. I. S. Pinto, Engineering Faculty, University of Porto, Rua Dr. Roberto Frias, s/n, 4200-465 Porto, Portugal. Electronic mail: spinto@fe.up.pt

Numerical studies have been an auxiliary tool for the prevention and treatment for atherosclerosis disease.[2–16] They have been an effective method for assessing the pressure along the coronary artery,[4,30] evidencing its role in assisting medical procedures.

The right coronary artery (RCA) has a complex geometry whose hemodynamic behavior is dominated by its geometric configuration,[25] necessitating the use of geometric models as close as possible to the reality for simulations. The main RCA side branches—Sino-atrial (SA) node, Conus, Right-Ventricular (RV) and Acute Marginal (AM)—are neglected in many previously published numerical studies.[14–17,19,20,25,34,35,41] However, it is of great importance to consider the side branches, since they modulate the outflow to the myocardium[4,10,36,40] and greatly influence the ability to perceive pathological patterns in WSS.[10]

The compliance between the arterial wall and the lumen is often neglected due to the more complex computational model. Nevertheless, Torii *et al.*[35] found that the compliance significantly affects the distribution of the hemodynamic descriptors when comparing the compliant model with the static one, particularly in the distal region.[40] Moreover, few studies[34,41] concluded that the dynamic cardiac motion has significant effects in instantaneous WSS values.

The present work goes further in assessing a statistically relevant study of several RCA geometric parameters—ostium cross-sectional area; angles between the RCA and the side-branches; tortuosity, curvature and cross-sectional area in each side-branch—and their influence in establishing hemodynamic conditions favorable to atheroma formation, through the analysis of the hemodynamic descriptors. Simulations, to obtain hemodynamic parameters, were performed through a compliant model between the arterial wall and blood, Fluid–Structure Interaction (FSI), with physiologically realistic boundary conditions.

MATERIALS AND METHODS

Study population

From a population of symptomatic patients referred to Coronary CT Angiography at Gaia/Espinho Hospital Centre, 10 male individuals with mean age of 35.1 ± 5.17, good image quality, right coronary dominance and absence of coronary atherosclerosis were selected (Fig. 1). These individuals have presented a total absence of any calcification (Agatston Calcium Score = 0), and absence of any non-calcified plaque or luminal irregularity. All subjects gave informed consent and the present research was approved by the institutional ethical committee.

CT Acquisition Technique

All CT examinations were performed with a third-generation 2 × 192-section dual-source CT system (SOMATOM Force; Siemens Healthcare Sector, Forchheim, Germany). Before the coronary CT angiography study, a nonenhanced prospectively ECG-triggered high-pitch spiral CT acquisition was performed in all patients to obtain the coronary calcium score.

Optimal timing for acquisition start was determined by using a test-bolus protocol. A volume of 50–80 mL of Iopromide (Ultravist 370; Bayer Pharma AG, Berlin, Germany) as injected at a flow rate of 5–6 mL/s through an 18-gauge intravenous antecubital catheter, followed by a saline flush at the same flow rate. All coronary CT angiography data sets were acquired by using prospectively ECG-triggered high-pitch spiral acquisition during diastole. The mean effective radiation dose was 1.103 ± 0.3065 mSv.

Segmentation, Model Definition and Mesh Generation

All contrast-enhanced coronary CT angiography data were reconstructed with a section thickness of 0.6 mm in the axial plane, using a third-generation iteractive reconstruction technique (advanced modeling iterative reconstruction, or ADMIRE; Siemens Healthcare Sector).

Then, the CT scans were analyzed through the commercial software Mimics®. The semi-automatic algorithm implemented in the software allows reconstructing the arterial lumen through the manual selection of the Aorta domain and the RCA points of interest (ostium and multiple side-branches). Once the ostium and all the visible side-branches have been manually selected, the implemented algorithm adjusts the coronary path and its lumen area to produce a tri-dimensional mask of the RCA model (Fig. 2a). The adjustment is based on the intensity deviation from the selected points. Only vessels with a radius greater than 0.5 mm were considered to be of interest. The proximal segment (segment with the highest radius) was successfully captured in all models with a maximum segmentation radius of 3 mm. The tri-dimensional mask was processed in order to produce a smooth model of the lumen. The arterial wall domain was reconstructed extruding outwards the fluid domain by 0.5 mm (H = 0.5 mm), value according to Guerciotti *et al.*[12] and Friedmand *et al.*[43]

The RCA models were discretized using Meshing Ansys® software with tetrahedral elements for both structural and fluid domains (10 and 4 nodes, respectively). A virtual topology and a patch independent method were used, since the tri-dimensional models are

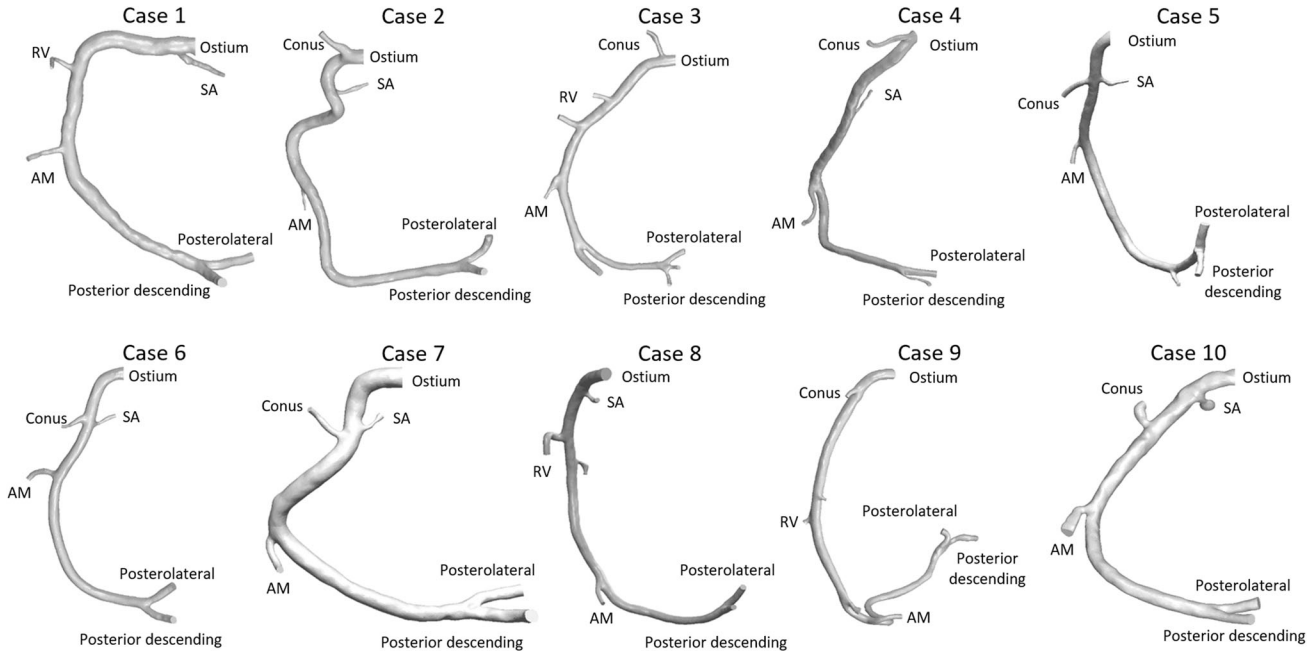

FIGURE 1. ***In-vivo*** **reconstructed models of the RCA based on CT scans (Siemens SOMATOM Force®, Erlanger, Germany) provided by the Cardiology Department of Gaia/Espinho Hospital Centre.**

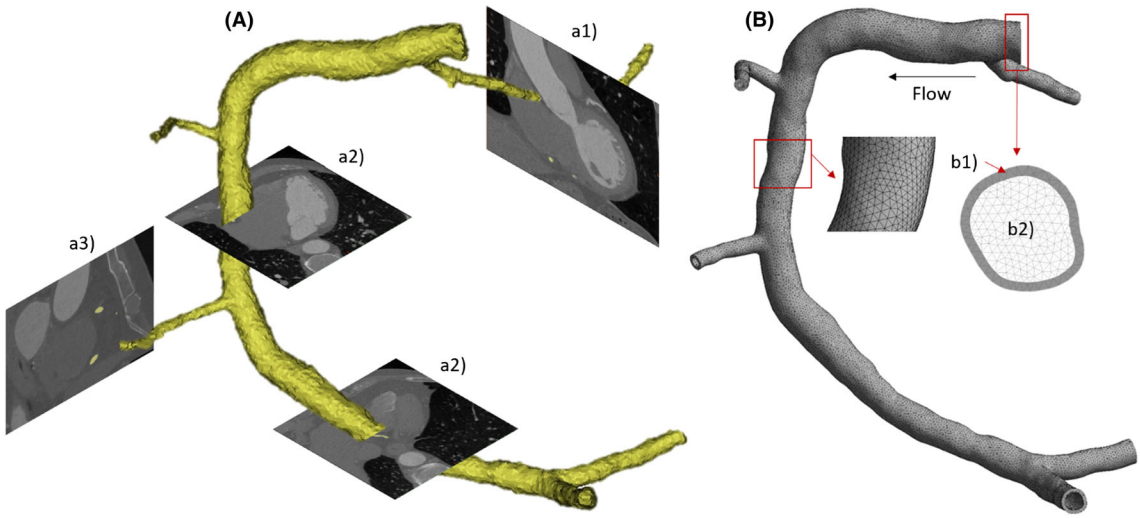

FIGURE 2. (a) Schematic representation of the segmentation process of individual 1. The tri-dimensional mask results from the segmentation of each image slice, from each imaging plane: (a1) coronal; (a2) axial; (a3) sagittal. (b) Sample of an arterial wall mesh, individual 1. In detail, (b1) mesh of the arterial wall; (b2) mesh of fluid domain.

composed by hundreds of small facets. This method prevents nodal clusters and hence improves the overall quality of the mesh. The mesh quality was examined through the maximum Skewness of the elements. A maximum Skewness value equal to 0 indicates an equilateral cell—the best case scenario. A maximum *Skewness* value equal to 1 indicates a completely degenerated cell.[1] The accuracy of the mesh is achieved by combining a lower maximum Skewness (lower than 0.9 is acceptable) and a reasonable computational time.[26] In general, $452735 \pm 36\ 111$ tetrahedral elements were considered for the fluid domain (blood) with a maximum Skewness of 0.625 ± 0.043. Also, around 87118 ± 14080 tetrahedral elements were considered for the structural domain (arterial wall) with a maximum Skewness of 0.885 ± 0.021.

A constructed mesh for one case study, individual 1, is shown in Fig. 2b. The differences between the two

different domains, fluid (blood) and structural (arterial wall), are clearly visible.

Blood and Wall Properties

A non-Newtonian model provides a more detailed WSS distribution than the most commonly used Newtonian model.[3,28] Thus, blood was considered as an isotropic, incompressible, homogeneous and non-Newtonian fluid, with the shear-thinning property accordingly to Carreau model. The model fits blood experimental data well[28] and is, mathematically, modeled[29,42] by

$$\mu_f = \mu_\infty + (\mu_0 - \mu_\infty)\left[1 + (\lambda\dot{\gamma})^2\right]^{(n-1)/2} \quad (1)$$

where μ_f is the blood viscosity and $\dot{\gamma}$ the shear rate. The constant values of the model[29] are summarized in Supplementary Table 2. Moreover, blood was considered to have a constant density, ρ_f, equal to 1060 kg m^{-3}.[29]

Regarding the structural domain (arterial wall), isotropic, homogeneous, incompressible and non-linear hyperelastic material was considered. The non-linear hyperelastic material was defined by the 5-parameters Mooney–Rivlin.[18] The constitutive equation[9] is described as follows:

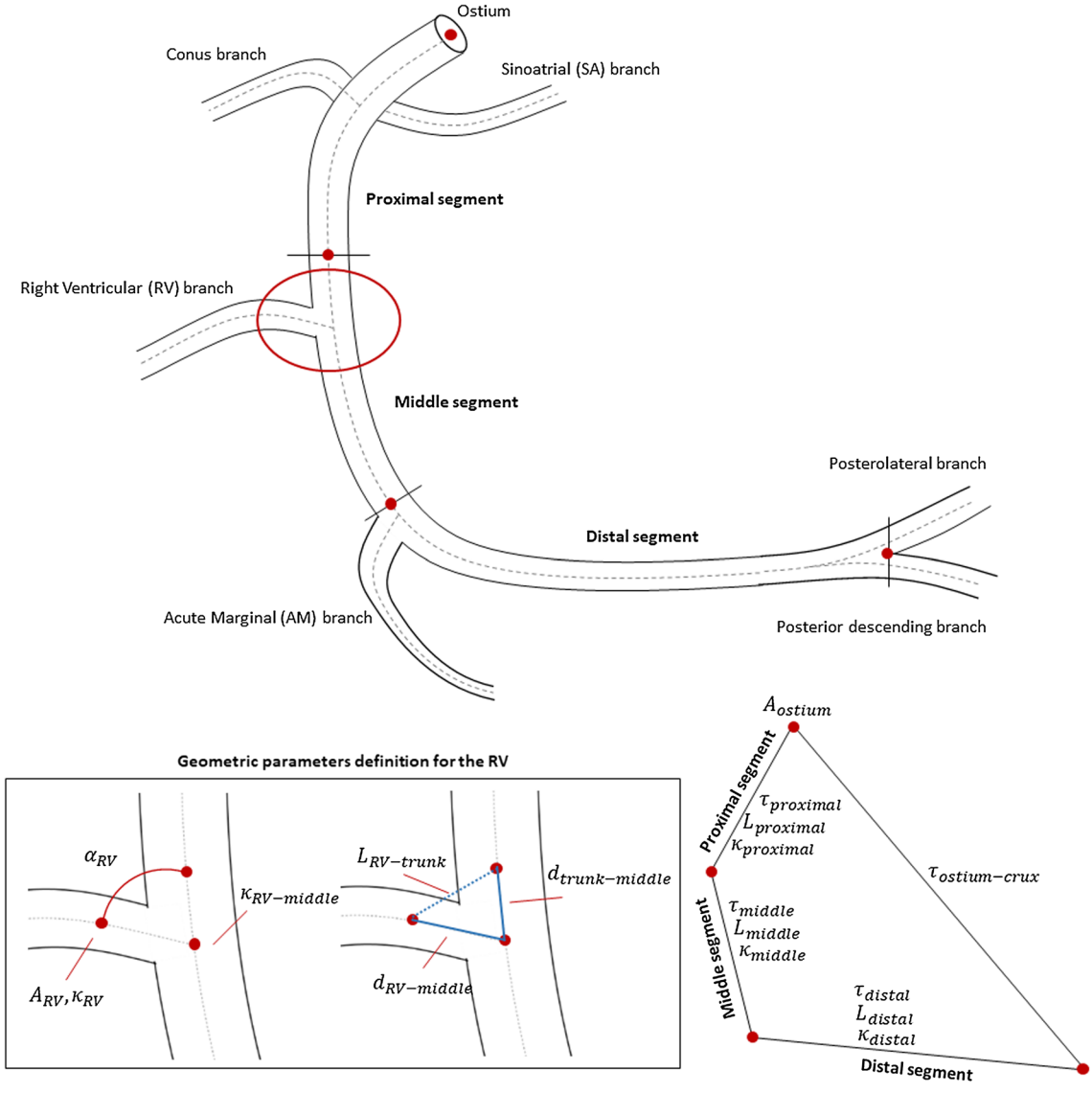

FIGURE 3. Measured geometric parameters in a RCA. For each side-branch, the geometric parameters were defined as shown for the Right Ventricular (RV) branch.

$$W = a_{10}(I_1 - 3) + a_{01}(I_2 - 3) + a_{20}(I_1 - 3)^2 + a_{11}(I_1 - 3)(I_2 - 3) + a_{02}(I_2 - 3)^2 + \frac{1}{d}(J - 1)^2 \quad (2)$$

where W represents the strain energy–density function, I_1 and I_2 the first and second strain invariants and J the elastic volume ratio. The constant values[18] of the constitutive equation are described in Supplementary Table 3. Furthermore, the arterial wall was considered to have constant density, ρ_w, equal to 1120 kg m^{-3}.[9]

Fluid–Structure Interaction Method

The Fluid–Structure Interaction (FSI) method was implemented in Workbench Ansys® package software. FSI simulation method is important to consider, since differences assuming deformable wall or rigid wall of the artery can be observed by Pinho *et al.*[26,27] The algorithm of FSI solves both fluid and solid domain separately. Once the fluid domain has been calculated and converged, the resulting forces across the outermost nodes in the fluid domain, which physiologically represents the endothelium, are transferred to the innermost layer of the wall also representing the endothelium. Then, the resulting displacements are calculated. When the solution has been converged in the structural domain and in the fluid–structure interfaces, the fluid mesh is updated through a diffusion based smoothing method.

In the fluid domain, the time step size considered was 0.005 s/time step, the number of iterations for each time step was 20 and the time step number defined was 444, corresponding to the time of three cardiac cycles (3 cardiac cycles × 0.74 s/cardiac cycle = 2.22 s). In each time step, a minimum of 10 and maximum of 30 coupling steps (or sub-iterations) was stipulated in the structural domain. The convergence in the structural domain was obtained when the difference between two coupling steps (or sub-iterations) is lower than 0.01. Then, the process is repeated for the following time step until completing the 444 time steps considered, corresponding to the time of three cardiac cycles.

In the fluid domain, Navier–Stokes equations are solved considering a laminar flow. Reynolds number in the systolic peak, maximum velocity, has a maximum of 970.[27,28] The velocity–pressure coupled equations were solved by SIMPLE algorithm[1] and the momentum equations were discretized by the second order upwind scheme.

The implemented FSI method was validated by Pinho *et al.*[26] in patient-specific carotid arteries, where the computed velocities acquired in discrete regions were compared with *in vivo* velocity measurements through Ultrasound Doppler scans provided by the medical team.

Boundary Conditions of the RCA

Torii *et al.*[35] measured the velocity and pressure time-dependent waveforms in the proximal segment of a patient with severe stenosis, using an intravascular ultrasound Doppler and pressure probe, respectively. Since the studied cases are of healthy individuals, the pressure arising from the stenosis should not be considered. Hence, the pressure waveform measured by Torii *et al.*[35] was manipulated, in order to exhibit the normal pressure of a cardiac pulse of a healthy individual (Supplementary Fig. 1). The pressure at the diastole, $p_{diastole}$, was considered equal to 80 mmHg and the pressure at the systole, $p_{systole}$, equal to 120 mmHg, corresponding to the normal pulse pressure range of healthy individuals.[7] Both the velocity and pressure waveform profiles were reconstructed through Fourier series using Matlab® software. Both profiles were further implemented into ANSYS CFX Command Language to define them as boundary conditions (Supplementary Fig. 1).

At the Ostium (inlet boundary condition), a Womersley velocity profile was imposed. The profile adapts, in space and time, the general Poiseuille profile accordingly to the vessel radius (R), the cardiac frequency (ω), the blood viscosity (μ_f) and the mean velocity magnitude (V_{in}^m). These conditions provide a better approximation to the fully developed velocity profile[32,38]:

$$v(r,t) = \frac{AR^2}{i\mu_f\alpha^2}\left(1 - \frac{J_0\left(i^{3/2}\alpha\frac{r_d}{R}\right)}{J_0(i^{3/2}\alpha)}\right)e^{i\omega t} \quad (3)$$

where the blood dynamic viscosity (μ_f) is equal to 0.00345 Pa s; r_d is the radial distance from the center of the artery to a given point inside the arterial wall; J_0 the first order Bessel function; $A = \frac{1}{\rho_f}\frac{\partial P}{\partial r}$ the pressure gradient, ρ_f the blood density and $\alpha = R\sqrt{\frac{\rho\omega}{\mu_f}}$ the Womersley number.

The Womersley number defines the velocity profile applied at the inlet surface. Values closer to 1 are associated to parabolic profiles, while higher values are associated to uniform profiles. Since the ostium surface is not a perfect circle, the Womersley number, for each individual case, was calculated considering the radius of an equivalent circle with the same area (Supplementary Table 4). The mean velocity magnitude at the inlet, V_{in}^m, measured in discrete time instant, is defined by the velocity waveform shown in Supplementary Fig. 1.

TABLE 1. Pearson correlation coefficients and *p*-value.

	Hemodynamic descriptors											
	Proximal			Middle			Distal			Global		
	$\bar{x}_{TAWSS}$	$\bar{x}_{OSI}$	$\bar{x}_{RRT}$	$\bar{x}_{TAWSS}$	$\bar{x}_{OSI}$	$\bar{x}_{RRT}$	$\bar{x}_{TAWSS}$	$\bar{x}_{OSI}$	$\bar{x}_{RRT}$	$\bar{x}_{TAWSS}$	$\bar{x}_{OSI}$	$\bar{x}_{RRT}$
A_{ostium}				0.66 (6.2e−4)		− 0.68 (5.8e−6)	0.82 (3.1e−3)		− 0.41 (6.0e−6)	0.74 (4.7e−3)		0.51 (5.86e−6)
$L_{proximal}$	− 0.55 (2.0e−5)			− 0.59 (1.8e−5)	0.47 (8.3e−9)					− 0.45 (3.2e−5)		
L_{middle}	− 0.55 (2.0e−5)			− 0.59 (1.8e−5)	0.47 (8.3e−9)					− 0.45 (3.2e−5)		
L_{distal}	0.55 (2.4e−5)			0.59 (2.4e−5)	− 0.47 (2.6e−8)	− 0.43 (4.0e−3)				0.45 (4.00e−5)		
$\tau_{ostium-crux}$					0.46 (2.2e−8)							
$\tau_{proximal}$								− 0.43 (7.8e−4)			− 0.41 (8.0e−4)	
$\kappa_{proximal}$												
τ_{middle}												
κ_{middle}				− 0.48 (1.4e−5)	0.52 (6.6e−6)	0.42 (3.0e−3)	− 0.45 (2.5e−4)			− 0.44 (2.6e−5)		
τ_{distal}								− 0.59 (8.0e−5)			− 0.51 (8.2e−5)	
κ_{distal}								− 0.54 (2.1e−6)				
α_{SA}	0.49 (1.5e−9)	− 0.55 (1.5e−8)	− 0.44 (1.5e−8)		− 0.50 (1.5e−8)						− 0.71 (1.5e−8)	
τ_{SA}		0.43 (3.2e−7)		0.50 (2.0e−5)			0.49 (3.3e−4)	0.72 (3.4e−7)			0.57 (3.5e−7)	
κ_{SA}	0.86 (2.1e−5)	− 0.48 (1.1e−3)		0.63 (1.9e−5)			0.45 (3.3e−4)	− 0.47 (1.0e−3)		0.59 (3.4e−5)	− 0.51 (1.1e−3)	
$\kappa_{SA-proximal}$												
A_{SA}		0.87 (7.7e−4)	0.76 (1.8e−3)					0.92 (7.7e−4)	0.74 (2.8e−3)		0.88 (7.7e−4)	0.62 (2.3e−3)
α_{conus}	0.41 (2.1e−7)	− 0.43 (2.4e−7)			− 0.42 (2.4e−7)			− 0.62 (2.4e−7)		0.44 (2.3e−7)	− 0.51 (2.4e−7)	
τ_{conus}								0.69 (1.9e−4)			0.48 (1.9e−4)	
κ_{conus}				− 0.51 (1.7e−5)	0.63 (4.1e−3)							
$\kappa_{conus-proximal}$												
A_{conus}												
α_{RV}				− 0.98 (1.7e−3)	0.72 (1.5e−3)	0.97 (1.5e−3)	− 0.97 (1.6e−3)			− 0.99 (1.8e−3)		0.61 (1.5e−3)

TABLE 1. continued.

	Hemodynamic descriptors											
	Proximal			Middle			Distal			Global		
	$\bar{x}_{TAWSS}$	$\bar{x}_{OSI}$	$\bar{x}_{RRT}$	$\bar{x}_{TAWSS}$	$\bar{x}_{OSI}$	$\bar{x}_{RRT}$	$\bar{x}_{TAWSS}$	$\bar{x}_{OSI}$	$\bar{x}_{RRT}$	$\bar{x}_{TAWSS}$	$\bar{x}_{OSI}$	$\bar{x}_{RRT}$
τ_{RV}				0.99 (1.8e−5)	− 0.66 (2.0e−2)		0.98 (3.0e−4)			0.98 (3.0e−5)		
κ_{RV}				0.47 (1.6e−5)			0.45 (2.9e−4)			0.65 (3.0e−5)		
$\kappa_{RV-middle}$				− 0.49 (1.5e−5)			− 0.44 (2.6e−4)	− 0.74 (3.9e−2)	− 0.66 (1.4e−2)		− 0.86 (3.9e−2)	− 0.46 (1.3e−2)
A_{RV}					− 0.73 (2.7e−2)	− 0.48 (2.7e−4)			− 0.88 (4.2e−2)		− 0.47 (2.7e−2)	− 0.84 (4.0e−2)
α_{AM}							− 0.46 (8.6e−8)			− 0.45 (1.1e−7)		
τ_{AM}							0.56 (2.8e−4)			0.57 (2.9e−5)		
κ_{AM}												
$\kappa_{AM-distal}$												
A_{AM}												0.43 (3.0e−4)

At the multiple outlet branches, a uniform, radius-independent and time-dependent, pressure profile was imposed (Supplementary Fig. 1). Since the tri-dimensional models were reconstructed through CT scans acquired at diastolic phase, the corresponding pressure must be offset.[35] Therefore, the computed pressure profile, $P(t)$, is described as follows:

$$P(t) = p(t) - p_{\text{diastole}} \tag{4}$$

where $p(t)$ is the manipulated pressure profile corresponding to a healthy pulse pressure[35] and p_{diastole} the diastolic pressure. To prevent flow reflux, the minimal pressure was set to 1 mmHg, maintaining the vessels pressurized all the time.

Hemodynamic Descriptors

Some authors, such as Malek *et al.*,[23] have linked the low WSS with the disturbed flow to find atherosusceptible regions. This behavior is well captured when analyzing the WSS-based hemodynamic descriptors.[28,32,33,42] The descriptors provide a single metric, summarizing the hemodynamic behavior along the cardiac cycle. They are based on the total time of the cardiac cycle, T; the location in the artery, s; and the instant time, t. The most commonly used WSS hemodynamic descriptors are the time average wall shear stress (TAWSS), the oscillatory shear index (OSI), and the relative resident time (RRT).

The TAWSS evaluates the mean value of the WSS magnitude ($WSS = \sqrt{WSS_x^2 + WSS_y^2 + WSS_z^2}$) along the cardiac cycle. Lower values of TAWSS, below 0.4 Pa, have indicated higher bias to plaque formation.[23]

$$TAWSS(s) = \frac{1}{T}\int_0^T |\text{WSS}(s,t)|\text{d}t \tag{5}$$

The OSI measures the disturbed flow near the wall along the cardiac cycle. The dimensionless parameter ranges from 0 (no flow oscillation) to 0.5 (highly disturbed flow with a 180º flow deflection).[13,31]

$$OSI(s) = 0.5\left[1 - \left(\frac{\left|\int_0^T \text{WSS}(s,t)\right|}{\int_0^T |\text{WSS}(s,t)|}\right)\right] \tag{6}$$

The RRT descriptor indicates the residence time of the particles near the arterial wall and is thought to be the most reliable metric to assess blood flow disruptions.[21] This metric is directly dependent on the OSI and inversely dependent on the TAWSS. High RRT values are correlated with the increase of disturbed flow (OSI) and with the decrease of WSS. Gallo *et al.*[8]

suggest that RRT values greater than 8 Pa^{-1} show susceptible regions to atherosclerosis appearance in the near-wall vicinity.

$$\mathrm{RRT}(s) = \frac{1}{(1 - 2 \cdot \mathrm{OSI}) \cdot \mathrm{TAWSS}} \tag{7}$$

Geometric Parameters

The following geometric parameters (see Fig. 3) were measured for all the RCA cases:

- The cross-sectional area of the ostium, A_{ostium};
- The dimensionless length of each segment, L_{segment};
- The tortuosity between the ostium and the crux, $\tau_{\mathrm{ostium-crux}}$;
- The tortuosity between the extreme points of each segment, τ_{segment};
- The mean curvature measured in each segment, $\kappa_{\mathrm{segment}}$;
- The cross sectional area at the beginning of each side-branch, A_{branch};
- The angle between each side-branch and the common trunk, α_{branch};
- The tortuosity between each side-branch and the common trunk, τ_{branch};
- The curvature between each side-branch and the segment, $\kappa_{\mathrm{branch-segment}}$;
- The curvature at the beginning of each side-branch, κ_{branch}

The tortuosity[24,39] was calculated as being the ratio between the shortest length, L_{i-j}, and the distance along the vessel centerline, d_{i-j}, calculated between two points of interest, i and j (see Fig. 3).

$$\tau = \left(1 - \frac{L_{i-j}}{d_{i-j}}\right) \tag{8}$$

The geometric information related to each side-branch was obtained from the centerline bifurcation to discrete points corresponding to two times the diameter of the sino-atrial. If the sino-atrial does not exist in the RCA, the conus branch diameter was considered instead of the sino-atrial. This metric was used in order to normalize each individual geometric measurements.

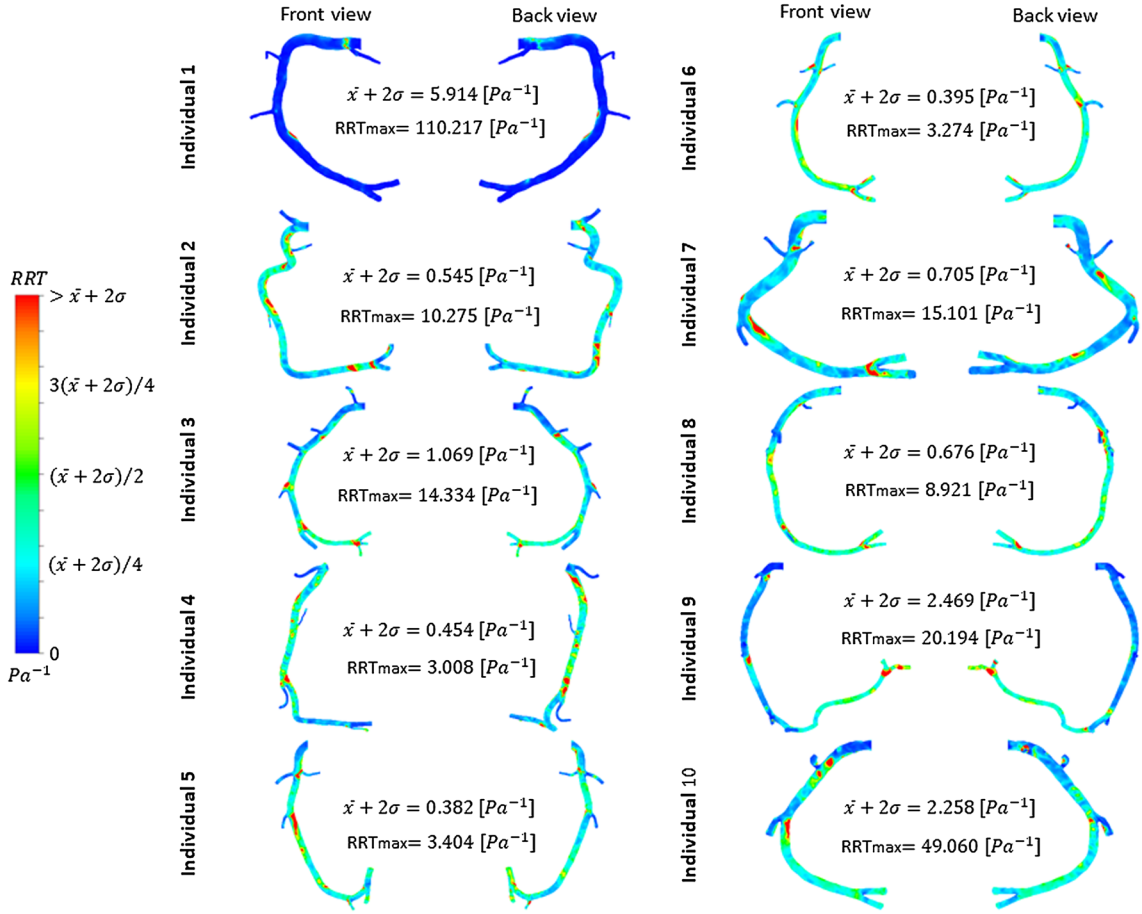

FIGURE 4. RRT distribution in the studied RCA cases including RRT maximum and top 2.5% of the distribution ($\bar{x} + 2\sigma$).

The values of the measured geometric parameter for each RCA case are presented in Supplementary Table 1. Both sino-atrial and conus branch were considered to be part of the proximal segment; the right-ventricular branch to be part of the middle segment; and the acute marginal to be part of the distal segment. The RCA cases do not present all the side-branches, depending on each specific case. Unfilled cells of Supplementary Table 1 represents the non-existence of a side-branch of a specific RCA case.

RESULTS

WSS Hemodynamic Descriptors for RCA Cases

RRT as a hemodynamic descriptor is a function of TAWSS and OSI, presenting the same distribution in the three parameters.[26,28,29] Since RRT is considered the strongest metric for assessing atherosclerotic plaque formation,[20] TAWSS and OSI were found unnecessary to be represented. In Fig. 4, the computed values of RRT, for each RCA model, range from 0 to $\bar{x} + 2\sigma$ Pa^{-1}—mean plus standard deviation. A normal distribution of RRT was considered and validated. Supplementary Table 5 shows that the percentage of RRT area higher than $\bar{x} + 2\sigma$ was 2.47%, following a normal distribution previously considered. For the same data, the normal probability plot was also calculated (Supplementary Fig. 2), showing a correlation coefficient of 0.919 (strong correlation—near 1).

Values equal to or higher than $\bar{x} + 2\sigma$ Pa^{-1} show a higher bias to a hemodynamic behavior associated with atherosclerotic plaque formation. This common metric ($\bar{x} + 2\sigma$) was applied in order to observe 97.5% of RRT values with greater resolution—zones between blue and red of Fig. 4. Moreover, RRT regions higher than 2.5%, atherosusceptible regions, are represented by red zones. A tendency for the increase of RRT along the RCA common trunk is also observed. RRT increases approximately 52% from the proximal segment to the distal segment, for all the RCA models. The mean RRT in the proximal segment is 0.240 ± 0.142 Pa^{-1}, in the middle segment is 0.268 ± 0.154 Pa^{-1} and in the distal segment is 0.363 ± 0.258 Pa^{-1}.

Furthermore, the mean mass flow rate repartition between each branch and the total mass flow was also determined. The mass flow rate in the crux is $43 \pm 22.2\%$, for all RCA cases. Approximately 57% of blood flows to the other side-branches. These values present the determinant role of the side-branches in the simulations. The outflow in these branches cannot be neglected, as concluded by Wellnhofer *et al.*[36]

Correlation Between Geometric Parameters and Hemodynamic Descriptors

A linear regression analysis was performed between all the considered geometric parameters of the RCA and the WSS hemodynamic descriptors—mean TAWSS, mean OSI and mean RRT in each segment and in the global RCA—in order to assess the relevance of the geometric parameters in the descriptors, and consequently, in hemodynamic behavior characteristic for atherosclerosis appearance. The correlation parameters presented in Table 1 are averaged for all patients. The commercially available software Microsoft Excel® was used to evaluate the associations, statistically.

The statistical relevance of all the considered RCA geometric parameters was assessed through Pearson correlation coefficient (r) and their significance through p-value.[24] The Pearson correlation coefficient depicts the extent that a change in one variable affects another variable. The Pearson correlation coefficient was calculated according to Evans.[6] $|r| \leq 0.20$ was considered a very weak correlation, $0.20 \leq |r| \leq 0.39$ a weak correlation, $0.40 \leq |r| \leq 0.59$ a moderate correlation, $0.60 \leq |r| \leq 0.79$ a strong correlation and $|r| \geq 0.8$ a very strong correlation.[6,21,24] Moreover, according to the Pearson correlation coefficient definition, the constant r can vary between -1 and 1. When the constant r is negative, the two variables are correlated in an opposite behavior, i.e., if one increases, the other one decreases. When the constant r presents a positive value, the two variables are correlated in a direct behavior, i.e., if one increases, the other also increases or if one decreases, the other one decreases.

Table 1 represents the Pearson correlation coefficient and the respective p-value under the predictor variables. Only correlations where $|r| > 0.4$ and p-value < 0.05[5] were considered; and only correlations between a side-branch and the respective downstream segments were taken into account. Moreover, WSS-based descriptors are related to the hemodynamic behavior by:

- TAWSS values are associated with WSS magnitude—with more detail, TAWSS evaluates the mean value of the WSS magnitude along the cardiac cycle;
- OSI values are associated with flow disturbance—with more detail, OSI measures the disturbed flow near the wall along the cardiac cycle;
- RRT values are associated to the direct atherosclerotic plaque formation predisposition—with more detail, RRT descriptor indicates the residence time of the particles near the arterial wall. Since the RRT is directly depen-

dent on the OSI and inversely dependent on the TAWSS, RRT is considered the most robust metric for assessing prone regions to atherosclerosis appearance.

DISCUSSION

The results of the present study are aligned with and in continuity of published studies; and, as far as we know, no other study in the literature has gone further than the present work. Mylers *et al.*[25] illustrated that the curvature of the RCA dominates hemodynamics. Liu *et al.*[22] concluded that the geometry of the curvature and the angulation of the side-branches have a significant effect on the WSS in the hemodynamic analysis of RCA´s and its relation with atherosclerosis lesions. Wellnhofer *et al.*[36] and Giannopoulos *et al.*[11] concluded that side-branches must not be neglected in numerical flow simulation studies after comparing hemodynamic results of patient-specific RCA´s considering side-branches and not considering side-branches. Malvé *et al.*[24] studied the correlation between the WSS amplitude and the bifurcation angles in the left coronary artery (LCA). Tortuosity between coronary branches can be used as a surrogate marker for the potential local risk factor for atherosclerosis. The previous conclusions to evaluate atherogenesis risk were obtained uniquely by the WSS and not by WSS hemodynamic descriptors.

All the studies cited previously take into account several simplifications in the numerical simulations. Simplified and smooth models of the RCA are not so real. Rigid wall of the artery, in CFD simulations, was considered and the compliance between the arterial wall and blood has significant effects in instantaneous WSS values.[34,40,41] TAWSS and OSI descriptors were also evaluated by Torii *et al.*[34] which ranges to evaluate atherogenesis risk varies in the same way as those of the present paper. Simplifications relative to the rheological property of blood, considering Newtonian fluid, were also introduced by other authors and, in reality, blood is a Non-Newtonian fluid.[14,15]

Thus, in the present work, non-simplified RCA models of ten healthy individuals are presented with the respective side-branches. The simulations were performed through a compliant model between the arterial wall and blood with physiological realistic boundary conditions. Blood was considered as a non-Newtonian fluid. In these conditions, the main goal is to assess a statistically relevant study of several RCA geometric parameters—ostium cross-sectional area, angles, tortuosity, curvature and cross-sectional area in each side-branch—and their influence in establishing hemodynamic conditions favorable to atheroma formation, through the analysis of the hemodynamic descriptors, going further than the available literature.

The following subsections present, with detail, the correlations between the geometric parameters of the RCA and the hemodynamic descriptors in the proximal segment of the RCA, in the middle segment, in the distal segment and in the global RCA, citing the alignment that already exists in the literature.

Noteworthy Correlations in the Proximal Segment

In the proximal segment, the RCA geometric parameters which have the highest influence in the hemodynamic behavior are the sino-atrial curvature and its cross-sectional area. Strong correlations were found between WSS-based hemodynamic descriptors and the sino-atrial curvature and its cross-sectional area. A decrease in the κ_{SA} leads to a low WSS amplitude ($r = 0.86$) and a more disturbed flow ($r = -0.48$) which, consequently, leads to hemodynamic conditions more susceptible to atherosclerosis formation in this segment. These results are aligned with and in continuity of published studies.[22,25] Moreover, an increase in the A_{SA} is strongly correlated with the increase in the disturbed flow ($r = 0.87$), which originates hemodynamic conditions propitious for atherosclerotic plaque formation in the proximal segment ($r = 0.76$).

In contrast, no noteworthy correlations were found between the geometric parameters of the conus branch and the WSS hemodynamic descriptors. Therefore, the conus branch does not influence the atherosclerosis appearance in the proximal segment.

Noteworthy Correlations in the Middle Segment

The inlet area of the artery, expressed as A_{ostium}, is positively correlated with the WSS magnitude ($r = 0.66$), showing that a decrease in the area reduces the WSS magnitude from the proximal to the middle segment. This is due to the presence of branching arteries in the proximal and middle segments that reduce the flow rate through the middle segment, resulting in a reduction of WSS compared to the proximal segment before branching. Thus, it increases the bias to atherosclerotic plaque formation ($r = -0.68$) in the middle segment. The κ_{SA} is positively correlated with the WSS magnitude ($r = 0.63$), meaning that a decrease in the κ_{SA} leads to a low WSS amplitude, allowing a hemodynamic behavior susceptible to atherosclerosis formation. These results are in following of available literature.[22,25]

Moreover, the conus branch influences the hemodynamic behavior in the middle segment. An increase

of the κ_{conus} results in increasing the asymmetry of the velocity profiles at that region. Thus, the regions of inner and outer curvature would experience markedly velocity gradients and so very different WSS. Essentially, one wall would experience a reduction of WSS while the other would experience an increase in WSS due to the asymmetry. Then, this also influence OSI in those regions. In the present study, for these patient-specific cases, the decrease of the WSS magnitude is higher than the increase of WSS in the asymmetry ($r = -0.51$). Consequently, the increase of the disturbed flow is higher than the decrease in those regions of curvature of the conus ($r = 0.63$), leading to favorable atherogenic conditions in this segment.

The right ventricular branch seems to have a high influence on the hemodynamic in the middle segment. An increase in α_{RV} was found to decrease the WSS magnitude ($r = -0.98$), increase the disturbed flow ($r = 0.72$) and ultimately increase the hemodynamic conditions susceptible to plaque formation ($r = 0.97$). On the other hand, a decrease in τ_{RV} also leads to a lower WSS ($r = 0.99$) and a higher disturbed flow ($r = -0.66$). Moreover, a decrease in the cross-sectional area of the right-ventricular branch increases the hemodynamic disturbance—explained by the negative correlation ($r = -0.73$).

Noteworthy Correlations in the Distal Segment

In the distal segment, smaller A_{ostium} also provides lower WSS values ($r = 0.82$). A decrease in the area leads to a reduction of WSS magnitude from the middle to the distal segment. Once more, the presence of branching arteries in the middle and distal segments reduces the flow rate through the distal segment, which can result in a reduction of WSS compared to the middle segment before branching. This process leads to a predisposition to hemodynamic behavior related to plaque formation ($r = -0.41$). An increase in the sino-atrial tortuosity ($r = 0.72$) and in its cross-sectional area ($r = 0.92$) induces a more disturbed flow which is directly correlated with hemodynamic conditions that may lead to atherosclerotic plaque formation ($r = 0.74$). The conus branch also influences the hemodynamic behavior in the distal segment. The flow is more disturbed when the α_{conus} ($r = -0.62$) decreases and/or the τ_{conus} increases ($r = 0.69$).

The correlation coefficients found for the right-ventricular branch indicate the predominant role in describing hemodynamic behavior in the distal segment. An increase of the α_{RV} ($r = -0.97$) and/or a decrease of the τ_{RV} ($r = 0.98$) are strong conditions linked to a decrease of the WSS amplitude, which is crucial for future atheroma formation. Moreover, a decrease in both $\kappa_{RV-middle}$ ($r = -0.66$) and A_{RV} ($r = -0.88$) are associated with an increase in the favorable hemodynamic conditions to atherosclerotic plaque formation. These results go further than those of the published literature.[22,25]

In contrast, no noteworthy correlations were found between the WSS hemodynamic descriptors and the geometric parameters of the acute marginal branch. Thus, the acute marginal branch has no influence in atherogenic conditions in the distal segment.

Noteworthy Correlations in the Global RCA

The correlations between the WSS-based descriptors and the geometric parameters, represented in Table 1, were computed for the global RCA in order to observe concordances relative to the results for each segment. As described for both middle and distal segments, a decrease in A_{ostium} leads to a global decrease in the WSS magnitude ($r = 0.74$). A decrease in the area leads to a reduction of WSS magnitude from the proximal to the distal segment. The presence of branching arteries in the proximal, middle and distal segments reduces the flow rate through the distal segment, which can result in a reduction of WSS compared to the proximal and middle segment before branching. Although not analyzed in the segmented branches, a decrease in the α_{SA} shows to be harmful, creating a more disturbed flow ($r = -0.71$). As demonstrated in the proximal and distal branches, when the cross-sectional area A_{SA} increases, the disturbed flow also increases ($r = 0.88$) and the tendency for producing a hemodynamic behavior related to atherosclerotic plaque formation is higher ($r = 0.62$).

As detailed in the middle and distal segments, the right-ventricular branch shows a prevailing role in the hemodynamic behavior. Higher values of α_{RV} are strongly correlated with lower values of WSS magnitude ($r = -0.99$) and, consequently, higher predisposition for plaque formation ($r = 0.61$). The correlations between the hemodynamic descriptors and the τ_{RV} and κ_{RV} show a different progression. Lower values of tortuosity ($r = 0.98$) and curvature ($r = 0.65$) are associated with lower WSS magnitude, favoring atherogenesis.

The same conclusions were inferred for the geometric parameters $\kappa_{RV-middle}$ and A_{RV}. A decrease in their values leads to a more disturbed flow ($r = -0.86$ and $r = -0.47$, respectively) and an increase in the risk of atherosclerotic plaque formation ($r = -0.46$ and $r = -0.84$, respectively). These correlations show great advances relative to the available published studies.[22,25]

No noteworthy correlations were found between the WSS hemodynamic descriptors and the geometric

parameters of the conus and the acute marginal branches in the whole RCA.

Study Limitations

Although the study demonstrates possible relations between several geometric parameters of the RCA and favorable hemodynamic conditions promoting atherosclerotic plaque formation (increasing the RRT hemodynamic descriptor), some limitations exist. The CT scan images are not speckle-free, leading to a need for vessel smoothing due to the high roughness arising from the segmentation process. A constant arterial wall thickness was imposed, which may cause overdimension in the downstream (middle and distal) segments and also the side branches, tending for an increase in their stiffness. In addition, the constitutive model used to describe the arterial wall, as a non-linear hyperelastic material, was the 5-parameters Mooney–Rivlin,[18] commonly used by other authors, for coronary arteries. Nevertheless, other constitutive models could be applied which can influence the results. Moreover, the motion of the heart, expansion and contraction, which can affect the flow in coronary arteries, was not taken into account. Due to the large motion of the ventricles, inertia can play an important role in coronary blood flow, and induce further asymmetry in the velocity profiles and hence in the WSS. However, these limitations are considered acceptable to the performed statistical study, since the limitations are for all patient-specific cases and all the imposed realistic approaches go further than approaches from the available literature.

CONCLUSIONS

The correlations between the geometric parameters of the RCA and hemodynamic descriptors in the proximal segment of the RCA, in the middle segment, in the distal segment and in the global RCA, establishes the knowledge of hemodynamic conditions propitious to atheroma formation, going further than the available literature.

The strongest correlations were found in the middle and distal segments of the RCA. A decrease in the ostium area promotes a decrease in the WSS magnitude from the proximal to the distal segment. The presence of branching arteries in the proximal, middle and distal segments reduces the flow rate through the distal segment, which can result in a reduction of WSS compared to the proximal and middle segment before branching. A hemodynamic behavior associated with a higher predisposition for atherosclerotic plaque formation is emphasized in the distal segment. Very strong correlations were also achieved between geometric parameters—tortuosity, cross-sectional area, angle—of the right-ventricular branch and the WSS magnitude, in the middle and distal segments. The right-ventricular branch seems to influence the most the hemodynamic behavior in the right coronary artery. Lower values of tortuosity, smaller cross-sectional area and higher angle of the right-ventricular branch lead to hemodynamic conditions susceptible to atheroma formation, within the study cases.

In the future, authors intend to analyze the hemodynamics in patient-specific right coronary arteries with atherosclerosis. It is of great interest to verify, in a large sample of patients, if the location of the lesion is predominantly near the right ventricular branch. In this future study, the real arterial wall thickness should be imposed, for each patient, with other constitutive models describing the arterial wall.

ELECTRONIC SUPPLEMENTARY MATERIAL

The online version of this article (https://doi.org/10.1007/s13239-019-00403-8) contains supplementary material, which is available to authorized users.

ACKNOWLEDGMENTS

Authors gratefully acknowledge the financial support of the Foundation for Science and Technology (FCT), Portugal, the Engineering Faculty of University of Porto (FEUP), the Institute of Science and Innovation in Mechanical and Industrial Engineering (LAETA-INEGI), the Cardiovascular R&D Unit of the Medicine Faculty of University of Porto (FMUP) and the Cardiology Department of Gaia/Espinho Hospital Centre.

CONFLICT OF INTEREST

Authors declare that they have not any actual or potential conflict of interest.

ETHICAL APPROVAL

All procedures followed were in accordance with the ethical standards of the responsible committee on human experimentation (institutional and national) and with the Helsinki Declaration of 1975, as revised in 2000 (5).

INFORMED CONSENT

Informed consent was obtained from all patients for being included in the study.

REFERENCES

[1]Ansys® Academic Research 15.0. ANSYS Fluent Tutorial Guide., 2013.

[2]Bentzon, J. F., F. Otsuka, R. Virmani, and E. Falk. Mechanisms of plaque formation and rupture. *Circ. Res.* 114:1852–1866, 2014.

[3]Chaichana, T., Z. Sun, and J. Jewkes. Computational fluid dynamics analysis of the effect of plaques in the left coronary artery. *Comput. Math. Methods Med.* 2012:504367, 2012.

[4]Chu, M., C. von Birgelen, Y. Li, J. Westra, J. Yang, N. R. Holm, J. H. C. Reiber, W. Wijns, and S. Tu. Quantification of disturbed coronary flow by disturbed vorticity index and relation with fractional flow reserve. *Atherosclerosis* 273:136–144, 2018.

[5]Dahiru, T. P-value, a true test of statistical significance? A cautionary note. *Ann. Ibadan Postgrad. Med.* 6:21–26, 2011.

[6]Evans, J. D. Straightforward Statistics for the Behavioral Science. Boston: Brooks/Cole, 1995.

[7]Feher, J. Vascular Function: Hemodynamics BT—Quantitative Human Physiology (2nd ed.). Boston: Academic Press, pp. 568–577, 2012. https://doi.org/10.1016/B978-0-12-800883-6.00054-9.

[8]Gallo, D., G. Isu, D. Massai, F. Pennella, M. A. Deriu, R. Ponzini, C. Bignardi, A. Audenino, G. Rizzo, and U. Morbiducci. A survey of quantitative descriptors of arterial flows BT. In: Visualization and Simulation of Complex Flows in Biomedical Engineering, edited by R. Lima, Y. Imai, T. Ishikawa, and M. S. N. Oliveira. Dordrecht: Springer, 2014, pp. 1–24.

[9]Gao, H., Q. Long, M. Graves, J. H. Gillard, and Z. Y. Li. Carotid arterial plaque stress analysis using fluid-structure interactive simulation based on in vivo magnetic resonance images of four patients. *J. Biomech.* 42:1416–1423, 2009.

[10]Giannoglou, G. D., A. P. Antoniadis, Y. S. Chatzizisis, and G. E. Louridas. Difference in the topography of atherosclerosis in the left versus right coronary artery in patients referred for coronary angiography. *BMC Cardiovasc. Disord.* 10:2–7, 2010.

[11]Giannopoulos, A. A., Y. S. Chatzizisis, P. Maurovich-Horvat, A. P. Antoniadis, U. Hoffmann, M. L. Steigner, F. J. Rybicki, and D. Mitsouras. Quantifying the effect of side branches in endothelial shear stress estimates. *Atherosclerosis* 251:213–218, 2016.

[12]Guerciotti, B., C. Vergara, S. Ippolito, A. Quarteroni, C. Antona, and R. Scrofani. A computational fluid–structure interaction analysis of coronary Y-grafts. *Med. Eng. Phys.* 47:117–127, 2017.

[13]He, X., X. He, D. N. Ku, and D. N. Ku. Pulsatile flow in the human left coronary artery bifurcation: average conditions. *J. Biomech. Eng.* 118:74–82, 1996.

[14]Johnston, B. M., P. R. Johnston, S. Corney, and D. Kilpatrick. Non-newtonian blood flow in human right coronary arteries: steady state simulations. *J. Biomech.* 37:709–720, 2004.

[15]Johnston, B. M., P. R. Johnston, S. Corney, and D. Kilpatrick. Non-newtonian blood flow in human right coronary arteries: transient simulations. *J. Biomech.* 39:1116–1128, 2006.

[16]Kaazempur-Mofrad, M. R., and C. R. Ethier. Mass transport in an anatomically realistic human right coronary artery. *Ann. Biomed. Eng.* 29:121–127, 2001.

[17]Karimi, A., M. Navidbakhsh, S. Faghihi, A. Shojaei, and K. Hassani. A finite element investigation on plaque vulnerability in realistic healthy and atherosclerotic human coronary arteries. *Proc. Inst. Mech. Eng. Part H J. Eng. Med.* 227:148–161, 2012.

[18]Karimi, A., M. Navidbakhsh, A. Shojaei, K. Hassani, and S. Faghihi. Study of plaque vulnerability in coronary artery using Mooney-Rivlin model: a combination of finite element and experimental method. *Biomed. Eng. Appl. Basis Commun.* 26:1450013, 2014.

[19]Kirpalani, A., H. Park, J. Butany, K. W. Johnston, and M. Ojha. Velocity and wall shear stress patterns in the human right coronary artery. *J. Biomech. Eng. Asme* 121:370–375, 1999.

[20]Knight, J., U. Olgac, S. C. Saur, D. Poulikakos, W. Marshall, P. C. Cattin, H. Alkadhi, and V. Kurtcuoglu. Choosing the optimal wall shear parameter for the prediction of plaque location—A patient-specific computational study in human right coronary arteries. *Atherosclerosis* 211:445–450, 2010.

[21]Lee, S.-W., L. Antiga, and D. A. Steinman. Correlations among indicators of disturbed flow at the normal carotid bifurcation. *J. Biomech. Eng.* 131:061013, 2009.

[22]Liu, G., J. Wu, D. N. Ghista, W. Huang, and K. K. L. Wong. Hemodynamic characterization of transient blood flow in right coronary arteries with varying curvature and side-branch bifurcation angles. *Comput. Biol. Med.* 64:117–126, 2015.

[23]Malek, A. M., S. L. Alper, and S. Izumo. Hemodynamic shear stress and its role in atherosclerosis. *JAMA* 282:2035–2042, 1999.

[24]Malvè, M., A. M. Gharib, S. K. Yazdani, G. Finet, M. A. Martínez, R. Pettigrew, and J. Ohayon. Tortuosity of coronary bifurcation as a potential local risk factor for atherosclerosis: CFD steady state study based on in vivo dynamic CT measurements. *Ann. Biomed. Eng.* 43:82–93, 2014.

[25]Myers, J. G., J. A. Moore, M. Ojha, K. W. Johnston, and C. R. Ethier. Factors influencing blood flow patterns in the human right coronary artery. *Ann. Biomed. Eng.* 29:109–120, 2001.

[26]Pinho, N., M. Bento, L. C. Sousa, S. Pinto, C. F. Castro, C. C. António, and E. Azevedo. Patient-Specific Study of a Stenosed Carotid Artery Bifurcation Using Fluid–Structure Interactive Simulation BT—VipIMAGE 2017: Proceedings of the VI ECCOMAS Thematic Conference on Computational Vision and Medical Image Processing Porto, Portugal, Octob. edited by J. M. R. S. Tavares, and R. M. Natal Jorge. Cham: Springer International Publishing, 2018, pp. 495–503. https://doi.org/10.1007/978-3-319-68195-5_54.

[27]Pinho, N., C. F. Castro, C. C. António, N. Bettencourt, L. C. Sousa, and S. I. S. Pinto. Correlation between geometric parameters of the left coronary artery and hemodynamic descriptors of atherosclerosis: FSI and statistical study. *Med. Biol. Eng. Comput.* 2018. https://doi.org/10.1007/s11517-018-1904-2.

[28]Pinto, S., and J. B. L. M. Campos. Numerical study of wall shear stress-based descriptors in the human left coronary

artery. *Comput. Methods Biomech. Biomed. Eng.* 19:1443–1455, 2016.
[29]Pinto, S. I. S., J. B. L. M. Campos, E. Azevedo, C. F. Castro, and L. C. Sousa. Numerical study on the hemodynamics of patient-specific carotid bifurcation using a new mesh approach. *Int. J. Numer. Method. Biomed. Eng.* 34:e2972, 2018.
[30]Siogkas, P. K., M. I. Papafaklis, A. I. Sakellarios, K. A. Stefanou, C. V. Bourantas, L. S. Athanasiou, T. P. Exarchos, K. K. Naka, L. K. Michalis, O. Parodi, and D. I. Fotiadis. Patient-specific simulation of coronary artery pressure measurements: An in vivo three-dimensional validation study in humans. *Biomed Res. Int.* 2015, 2015.
[31]Soulis, J. V., and D. K. Fytanidis. Oscillating shear index, wall shear stress and low density lipoprotein accumulation in human RCAs. *Acad. Sci. USA* 32:867–877, 2010.
[32]Sousa, L. C., C. F. Castro, C. C. António, A. M. F. Santos, R. M. dos Santos, P. M. A. C. Castro, E. Azevedo, and J. M. R. S. Tavares. Toward hemodynamic diagnosis of carotid artery stenosis based on ultrasound image data and computational modeling. *Med. Biol. Eng. Comput.* 52:971–983, 2014.
[33]Sousa, L. C., C. F. Castro, C. C. António, J. M. R. S. Tavares, A. M. F. Santos, R. M. Santos, P. Castro, and E. Azevedo. Simulated hemodynamics in human carotid bifurcation based on Doppler ultrasound data. *Int. J. Clin. Neurosci. Ment. Health* 1(1–7):15, 2014.
[34]Torii, R., J. Keegan, N. B. Wood, A. W. Dowsey, A. D. Hughes, G. Z. Yang, D. N. Firmin, S. A. M. Thom, and X. Y. Xu. MR image-based geometric and hemodynamic investigation of the right coronary artery with dynamic vessel motion. *Ann. Biomed. Eng.* 38:2606–2620, 2010.
[35]Torii, R., N. B. Wood, N. Hadjiloizou, A. W. Dowsey, A. R. Wright, A. D. Hughes, J. Davies, D. P. Francis, J. Mayet, G.-Z. Yang, S. A. M. Thom, and X. Y. Xu. Fluid–structure interaction analysis of a patient-specific right coronary artery with physiological velocity and pressure waveforms. *Commun. Numer. Methods Eng.* 25:565–580, 2009.
[36]Wellnhofer, E., J. Osman, U. Kertzscher, K. Affeld, E. Fleck, and L. Goubergrits. Flow simulation studies in coronary arteries-impact of side-branches. *Atherosclerosis* 213:475–481, 2010.
[37]WHO. The Atlas of Heart Disease and Stroke. Geneva: WHO, 2010.
[38]Womersley, J. R. Method for the calculation of velocity, rate of flow and viscous drag in arteries when the pressure gradient is known. *J. Physiol.* 127:553–563, 1955.
[39]Zakaria, H., A. M. Robertson, and C. W. Kerber. A parametric model for studies of flow in arterial bifurcations. *Ann. Biomed. Eng.* 36:1515–1530, 2008.
[40]Zeng, D., E. Boutsianis, M. Ammann, K. Boomsma, S. Wildermuth, and D. Poulikakos. A study on the compliance of a right coronary artery and its impact on wall shear stress. *J. Biomech. Eng.* 130:041014, 2008.
[41]Zeng, D., Z. Ding, M. H. Friedman, and C. Ross Ethier. Effects of cardiac motion on right coronary artery hemodynamics. *Ann. Biomed. Eng.* 31:420–429, 2003.
[42]Zhang, Q., B. Gao, and Y. Chang. Effect of different rotational directions of BJUT-II VAD on aortic swirling flow characteristics: a primary computational fluid dynamics study. *Med. Sci. Monit.* 22:2576–2588, 2016.
[43]Zhu, H., and M. H. Friedman. Relationship between the dynamic geometry and wall thickness of a human coronary artery. *Arterioscler. Thromb. Vasc. Biol.* 23:2260–2265, 2003.